Geomechanics and Engineering, *Vol. 34, No. 4 (2023) 461-472*
https://doi.org/10.12989/gae.2023.34.4.461

Influence of specimen height on the shear behavior of glass beads in the direct shear test

Young-Ho Hong[1a], Yong-Hoon Byun[2b] and Jong-Sub Lee*[1]

[1]*School of Civil, Environmental and Architectural Engineering, Korea University, 145, Anam-ro, Seongbuk-gu, Seoul, 02841, Republic of Korea*
[2]*School of Agricultural Civil & Bio-Industrial Engineering, Kyungpook National University, 80, Daehak-ro, Buk-gu, Daegu, 41566, Republic of Korea*

(*Received April 17, 2023, Revised July 3, 2023, Accepted July 20, 2023*)

Abstract. A box scale affects the shear behavior of soils in the direct shear test. The purpose of this study is to investigate the scale effect on the shear behavior of dilative granular materials by testing specimens of different heights placed in a type C shear box. Experimental tests were performed on specimens composed of glass beads with different heights and equal initial void ratios. Results showed that the peak friction and dilation angles linearly increased with the specimen height; however, the residual friction angle remained relatively constant. Similarly, the shear stiffness increased with the specimen height, rapidly reaching its peak state. Height does not have a significant effect on the total volume changes; nevertheless, a high aspect ratio can be assumed to result in global and homogeneous failure. The results and interpretations may be used as reference for recommending shear box scale in direct shear tests.

Keywords: direct shear test; glass beads; scale effect; shear behavior; shear stiffness

1. Introduction

The scale effect renders accurate prediction of shear behavior difficult in various geotechnical engineering problems. For example, in the case of a shallow foundation, the bearing capacity or contact pressure measured at the same depth varies with the width. This implies that the scale of the foundation affects the shear behavior of the subsoil structure (Kögler and Scheidig 1938, Cerato and Lutenegger 2007). Small-scale footings may hinder the development of a shear zone, resulting in an overestimation of the internal friction angle of the ground. Conversely, the friction angle is low in a wide footing (Cerato and Lutenegger 2006). Consequently, in previous studies, a large friction angle was considered when estimating the bearing capacity of a shallow foundation if the foundation was narrow, whereas a low friction angle was considered when the foundation was wide (Scarpelli and Wood 1982, Vermeer 1990). Moreover, the scale effect must be considered to analyze the shear behavior in direct shear tests. Since Parsons investigated the foregoing in 1936, several researchers have evaluated the scale effect on the shear behavior in direct shear tests. Zhou *et al*. (2009) reported that the stress-strain relationship depends on the ratio of the shear box size to the particle diameter as well as on the intrinsic properties of the material (such as particle size distribution and friction angle). In addition, Palmeira and Milligan (1989) reported that the ratio of shear box size to particle size affects the thickness of the shear zone generated by the shearing process and the shear behavior after the peak shear strength.

According to ASTM D3080/D3080M-11, the minimum length (L) or width (W) of a square specimen should be 50 mm or not less than 10 times the maximum particle diameter (D_{max}). Moreover, the initial height (or thickness) of the specimen should exceed 12 mm or not be less than six times D_{max}. Finally, the height-to-length ratio (aspect ratio, H/L) must not exceed 0.5. The ASTM D3080 recommendations have received considerable attention. Accordingly, experimental tests and numerical analyses were performed shear boxes and particles of various sizes. Based on each result, several suggestions regarding the appropriate shear-box size were presented.

Based on experimental tests conducted using a long shear box, Scarpelli and Wood (1982) proposed that the length of the shear box should be greater than 100 times D_{50} (the mean particle diameter). Jewell and Wroth (1987) reported that the size had no effect on the internal friction angle when L/D_{max} was 50 or higher. Through an experimental blade rotation test, Stone and Wood (1992) derived $176D_{50}$ (176 times D_{50}) as the shear-box length. Jacobson *et al.* (2007) derived $58D_{50}$ as the shear-box length using a two-dimensional (2D) discrete element method (DEM). Deiminiat *et al.* (2022) reported that the minimum L/D_{max} value required to remove the scale effect is approximately 60. Cerato and Lutenegger (2006) revealed that the test results still depended on the size, even though a

*Corresponding author, Professor
E-mail: jongsub@korea.ac.kr
[a]Ph.D. Candidate
E-mail: lovelymalpoy@korea.ac.kr
[b]Associate Professor
E-mail: yhbyun@knu.ac.kr

ISSN: 2005-307X (Print), 2092-6219 (Online)

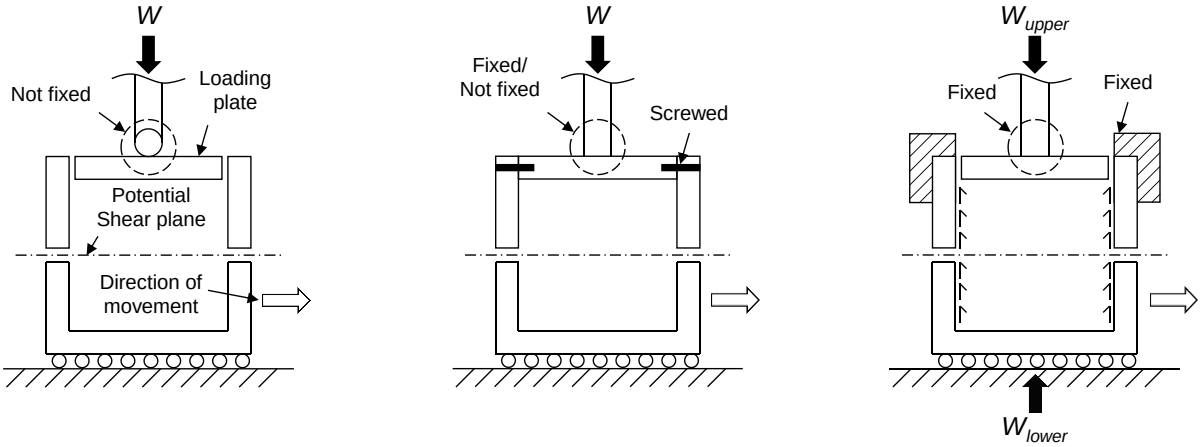

(a) Type A (b) Type B (c) Type C

Fig. 1 Three types of direct shear apparatus from Shibuya *et al*. (1997)

shear box satisfied the ASTM D3080 recommendations. Hence, they proposed that the largest available box should be used in experimental tests. Moreover, some have argued that the recommendations in ASTM D3080 regarding the shear box size must be reexamined. They insisted that box size recommendations should be increased to ensure that the specimen size does not affect shear behavior, including the friction angle results.

As previously mentioned, studies on the length-scale effect have been sufficiently conducted. In contrast, information regarding the height-scale effect on the shear behavior in direct shear tests is limited. In particular, the effect of height change with a constant length is not fully understood. Zhou *et al*. (2009) reported that, in some cases, the shear zone reached the upper boundary of the shear box, although the box size complied with the recommendations of ASTM D3080. Therefore, it is necessary to study the effect of the height scale in direct shear tests. Hight and Leroueil (2003) conducted direct shear tests using shear boxes of various sizes. They varied the height in the range of 50.8–154.9 mm; however, the box length was fixed at 254 mm. This indicates that the friction angle increased and the volume change decreased as the box height increased. Interpretations dealing with two problems, namely wall friction (between the specimen and the inner wall of the shear box) and the moment (of the specimen itself occurring during the shear process), have already been solved through several studies. Wang and Gutierrez (2010) analyzed the scale effect by varying the length and height in various ways using a 2D DEM. Two types of specimens were prepared using poorly graded and well-graded materials, with D_{50} equal to 0.7 mm. The experimental results indicated that when the specimen height was large, the number of particles involved in the shear process increased. Moreover, adding an external shear force to the peak strength resulted in global and uniform shear failure. In other words, if the specimen height is small, the stress and strain are localized, leading to progressive failure. In conclusion, for the direct shear test, the proposed minimum values of L/D_{max} and H/D_{max} are 60 and 40, respectively. Moreover, the proposed H/L is between 0.5 and 0.67; however, it does not agree with the maximum ratio being 0.5 or less, as recommended by ASTM D3080.

In a direct shear test, the volume change in the actual shear zone is generally known to be considerably greater than that measured at the boundary of the shear box. This is one of the major reasons for the relatively low H/L ratios recommended by the ASTM D3080 standards. The type of shear box also affects the shear behavior in the direct shear test, as elaborated in Section 2.1. To date, far, most experimental tests have been conducted using a conventional type-A shear box, and suggestions regarding box scale are based on this box type. Wang and Gutierrez (2010) suggested the use of a type-B shear box whose dimensions differed from those of the ASTM D3080 standard. This paper also describes the experimental investigations performed on type-C shear boxes with different heights. The effects of the height scale and shear-box type were examined through direct shear tests conducted on a dilative granular material. The types of shear boxes and their characteristics are presented, and the direct-shear apparatus used in this study is described in detail. The physical properties of the particle, specimen preparation methods, and test arrangements are explained. The analysis of the effect of the aspect ratio (H/L) on the resistance and deformation of the dilative materials was based on the experimental results. Furthermore, the stiffness characteristics were evaluated, and the influence of the specimen height on the total volume change and development of the shear zone was examined.

2. Direct shear testing device

2.1 Types of direct shear box

The shear behavior of soils in direct shear tests depends on whether each component of the shear box, including the loading plate, is fixed. As shown in Fig. 1, three types of direct shear boxes (DSBs) have been identified (Shibuya *et al.* 1997). Type A, devised by Skempton and Bishop (1950), is the most widely used type of DSB in direct shear tests. As

shown in Fig. 1(a), the loading plate and upper shear box are not fixed; they move freely and rotate independently. They tend to tilt and rotate owing to the moment induced by the load-transfer mechanism within the shear box. To avoid these problems, a type-B DSB with a symmetrical arrangement, in which the loading plate and upper shear box are rigidly fixed together to work as a single unit, has been proposed, as shown in Fig. 1(b) (Jewell and Wroth 1987). The symmetrical arrangement balances the applied load such that the rotation is reduced, and the deformation distribution may be more uniform on the shear plane (Jewell and Wroth 1987, Jewell 1989, Lings and Dietz 2004). However, the use of a type-B shear box does not seem to solve the fundamental drawbacks of a type-A box because the loading plate and upper shear box may rotate together. Moreover, maintaining a constant gap (i.e., opening) between the upper and lower shear boxes during the shearing process is difficult. If the opening is wide, particle outflow occurs, possibly decreasing the shear strength and hindering volume change. By contrast, if the opening is narrow, the development of a shear zone is suppressed, and the shear strength and volume change may be overestimated. Because of these problems, the reliability of the results obtained using a type-B DSB is uncertain.

Finally, the upper box and loading plate of the type-C shear box were rigidly and independently fixed, as shown in Fig. 1(c) (Mikasa 1960, Takada 1993). Note that a type-C DSB prevents the upper box from rotating or moving vertically and has a constant gap between the upper and lower shear boxes during the shearing process. By preventing horizontal movement and rotation of the loading plate, the volume change of the specimen can occur only in the vertical direction. Lings and Dietz (2004) improved a type-B shear box by attaching a pair of wings to the upper shear box to adjust and fix the opening size, which this is structurally similar to a type-C DSB. Owing to the wall friction between the inner walls of the shear box and the specimen generated by the volume change, the frictional force changed the vertical load acting on the shear plane such that the load differed from the vertical load applied to the top of the specimen. Shibuya *et al.* (1997) experimentally demonstrated that the vertical load should be measured at the bottom (W_{lower}) rather than at the top (W_{upper}) of the shear box to minimize the influence of wall friction and to measure the actual vertical stress applied to the shear plane.

2.2 Direct shear apparatus

A schematic of the direct-shear testing device used in this study is shown in Fig. 2. The upper shear box is fixed to the main frame, and the loading plate is fixed to the upper shear box. This box is the type-C shear box presented above. Two pairs of motors and load cells were installed, vertically and horizontally. The motors and load cells are located on the same side in the horizontal direction, whereas those in the vertical direction are located above and below the shear box. The upper shear box was separated from the lower box to ensure a constant opening. The loading plate was rigidly fixed (i.e., not hinged) to the motor in the vertical direction. The shear box was placed in a water tank with a transparent front wall. The water tank containing the lower shear box moved horizontally along the roller during shearing.

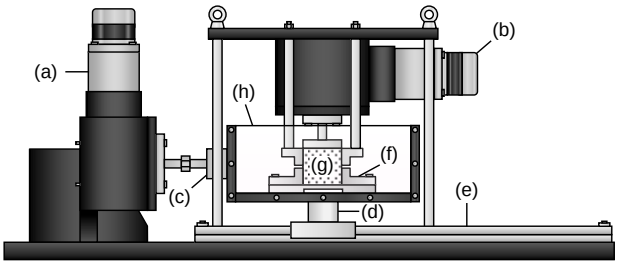

Fig. 2 Schematic drawing of the direct shear apparatus: (a)-(b) Motors, (c)-(d) Loadcells, (e) Roller way, (f) Shear box, (g) Soil specimen and (h) Water tank

A pair of α-step motors (AMR98AC-N50, Oriental Motor Co., Ltd.) was used to apply loads in the vertical and horizontal directions. A typical step motor has an open-loop system with a high response, and a servo motor exhibits high accuracy using a closed-loop system. The α-step motor combines the advantages of the step and servo motors, providing rapid response and accuracy. In addition to the high precision of 0.0072° per step, the α-step motor with a total gear ratio of 4500:1 and a combination of two gear boxes with ratios of 90:1 and 50:1 ensures that high torque and resolution are achieved. The travel distances of the vertical and horizontal motors can be determined using pulse input values. The applied loads in each direction are measured using replaceable load cells: a compressional canister load cell (CDES model, Bongshin Loadcell Co., Ltd.) and a binocular load cell (OBS263 model, Bongshin Loadcell Co., Ltd.). They have a load capacity of 100 kg and a maximum resolution of 1/10 000. The direction and speed of movement of the motors along each axis were automatically monitored and controlled in real-time.

The movements of the motors ensure stable performance, fast response, and small deviations through proportional-integral-differential (PID) control. Hardware and software operations, such as data acquisition and feedback processes, were automatically controlled using a LabVIEW-based program. Using this program, a user can set up and control the parameters (e.g., boundary condition, confining stress, and shear rate). Depending on the settings, the motor movements of the motors were determined using the numerically calculated nonlinear feedback of the PID control system in the program. The measured values monitored in real time were displayed, and the collected data (e.g., stress and displacement values) were saved in a text format file at every measurement interval.

2.3 DSB description

In this study, experimental tests were conducted using a shear box with a square cross-section rather than a circular one to evaluate the shear behavior of granular materials more accurately (Wu *et al*. 2008). The original size of the shear box was 80 mm × 80 mm × 70 mm (L × W × H), and the heights of the upper and lower shear boxes were 35 mm.

Table 1 Physical properties of the glass beads (SiLibeads® S-Type, Sigmund Lindner GmbH, Germany)

Property	Value
Specific gravity [-]	2.5
Hardness Mohs [-]	≥ 6
Roundness [%]	≥ 95
Young's modulus [GPa]	65
Particle size range [mm]	0.75–1.00
Maximum void ratio [-]	0.62
Minimum void ratio [-]	0.50

Steel plates with heights of 0, 5, 10, 15, and 20 mm were placed at the bottom of the shear box to adjust the height of the specimen. The heights of the specimens (70, 60, 50, 40, and 30 mm) correspond to aspect ratios (H/L) of 0.875, 0.75, 0.625, 0.5, and 0.375, respectively.

The shear strength and volume change were influenced by the opening size between the upper and lower boxes in the direct shear test (Kim *et al*. 2012, Lings and Dietz 2004, Kim 2021). If the opening is sufficiently wide to allow the particles to flow out, the shear strength and volume change decrease. In contrast, an extremely small opening can hinder the shear zone development, resulting in an overestimation of the shear strength and volume change. The glass beads (discussed in a later section) used in this study were highly vulnerable to particle outflow; consequently, the opening size suggested by Kim et al. (2012) was difficult to apply. Accordingly, in this study, the opening size was maintained at 0.4 mm to prevent particle leakage, which was regarded as the main priority.

3. Experimental setup

3.1 Physical properties of glass beads

The shear behavior of granular materials includes interparticle friction (due to particle roughness), spatial arrangement (due to particle shape), and interparticle locking. Glass beads were selected for this study because their round shape and poor grading diminished irregularities in particle shape and facilitated the repeated preparation of specimens under virtually the same conditions. The physical properties of the glass beads are listed in Table 1; the particle size is 0.75–1.00 mm. In terms of the scale of the shear box size, L/D_{max} was 80 and H/D_{max} was 30–70. The roundness of the glass beads was > 95%, and their hardness and elastic modulus were 6 or higher on the Mohs scale and 65 GPa, respectively, indicating their sufficient resistance to particle wear and breakage. To eliminate the influence of particle damage, the materials were not reused (i.e., single-use materials).

3.2 Specimen preparation

The specimens were prepared via dry fluviation and compaction. The glass beads were freely dropped from a constant height of 10 cm, and dry compaction was performed on each layer. The number of layers and compaction effort depend on the target specimen height and confining stress. Through trial and error, the initial void ratio (e_0) of the specimen was determined to be 0.540, which was obtained under all the experimental conditions. Here, e_0 refers to the void ratio of the specimen after the completion of consolidation, that is, before shearing. The e_0 error was limited to within ± 0.003; hence, the initial void ratios of all the specimens were equal for all tested specimens.

3.3 Test configuration

The specimens had five different heights (70, 60, 50, 40, and 30 mm), and the aspect ratios (H/L) were 0.875, 0.75, 0.625, 0.5, and 0.375. The experimental tests were conducted under constant pressure conditions with three confining stress values (σ'_v = 25, 50, and 100 kPa), which remained constant throughout the tests. For consolidation, the confining stress was first applied to the prepared specimen. Shearing is forced if the target initial void ratio is reached after settlement converges. All experimental tests were performed under an equal shear rate of 0.4 mm/min to eliminate the effect of shear rate on shear strength (Tika *et al.* 1996, Scaringi and Di Maio 2016, Beren *et al.* 2020). Shearing was performed until the shear displacement reached 12 mm, thereby ensuring a distinct residual strength with sufficient shear deformation.

4. Experimental results

The experimental results for different shear box heights are summarized in Table 2 and are shown in Fig. 3. The relationship between shear stress and shear displacement in Fig. 3(a) indicates that the peak shear strength increased with the aspect ratio (H/L). However, the residual strength was virtually constant, with no notable strain hardening or softening. Moreover, the height and confining stress did not affect the residual strength. An increase in the aspect ratio caused rapid attainment of the peak shear strength. With an increase in height, the shear displacement at the peak shear strength decreased. The plot of vertical displacement versus shear displacement in Fig. 3(b) indicates the occurrence of a slight initial contraction, followed by rapid expansion and a constant volume after a certain point. Furthermore, the greater the specimen height, the greater the absolute volume change. Based on these fundamental measurements from the direct shear test, the internal friction angles were derived from the Mohr-Coulomb failure envelope, as shown in Fig. 4. In Fig. 4(a), when the aspect ratio (H/L) is 0.375, the peak friction angle (ϕ'_{peak}) is 28.19°. The peak friction angles gradually increased with the aspect ratio. An angle of 37.18° was observed at an aspect ratio of 0.875, which differed considerably from the corresponding angle when the aspect ratio was 0.375.

To interpret the shear behavior of soils, determining the critical state after the peak strength is as important as obtaining the peak state. Casagrande (1936) established

Table 2 Experimental results from direct shear tests using different specimen heights and confining stresses

H/L [-]	σ'_v [kPa]	$(\tau/\sigma'_v)_{peak}$ [-]	$(\tau/\sigma'_v)_{res}$ [-]	ϕ'_{peak} [°]	ϕ'_{res} [°]	$\phi'_{peak} - \phi'_{res}$ [°]	ψ_{peak}* [°]	u_{peak}** [mm]	symbol
0.375	25	0.595	0.484	30.77	25.85	4.92	9.345	1.712	
	50	0.566	0.465	29.51	24.92	4.58	7.249	2.185	
	100	0.524	0.459	27.67	24.67	3.00	5.031	3.193	
0.5	25	0.611	0.500	31.43	26.57	4.86	12.83	1.577	
	50	0.588	0.486	30.44	25.92	4.52	10.95	1.983	
	100	0.577	0.457	30.00	24.57	5.43	11.08	1.779	
0.625	25	0.648	0.488	32.92	26.01	6.91	14.80	1.581	
	50	0.690	0.476	34.59	25.43	9.16	14.89	1.716	
	100	0.657	0.457	33.31	24.58	8.73	13.96	1.848	
0.75	25	0.720	0.502	35.75	26.63	9.11	17.14	1.107	
	50	0.689	0.450	34.58	24.25	10.33	15.28	1.579	
	100	0.682	0.453	34.29	24.39	9.90	15.03	2.187	
0.875	25	0.744	0.510	36.64	27.02	9.62	20.24	1.117	
	50	0.779	0.476	37.91	25.45	12.46	21.04	1.381	
	100	0.754	0.452	37.03	24.34	12.69	19.55	1.648	

*ψ_{peak}: dilation angle at peak stress ratio; **u_{peak}: shear displacement at peak stress ratio

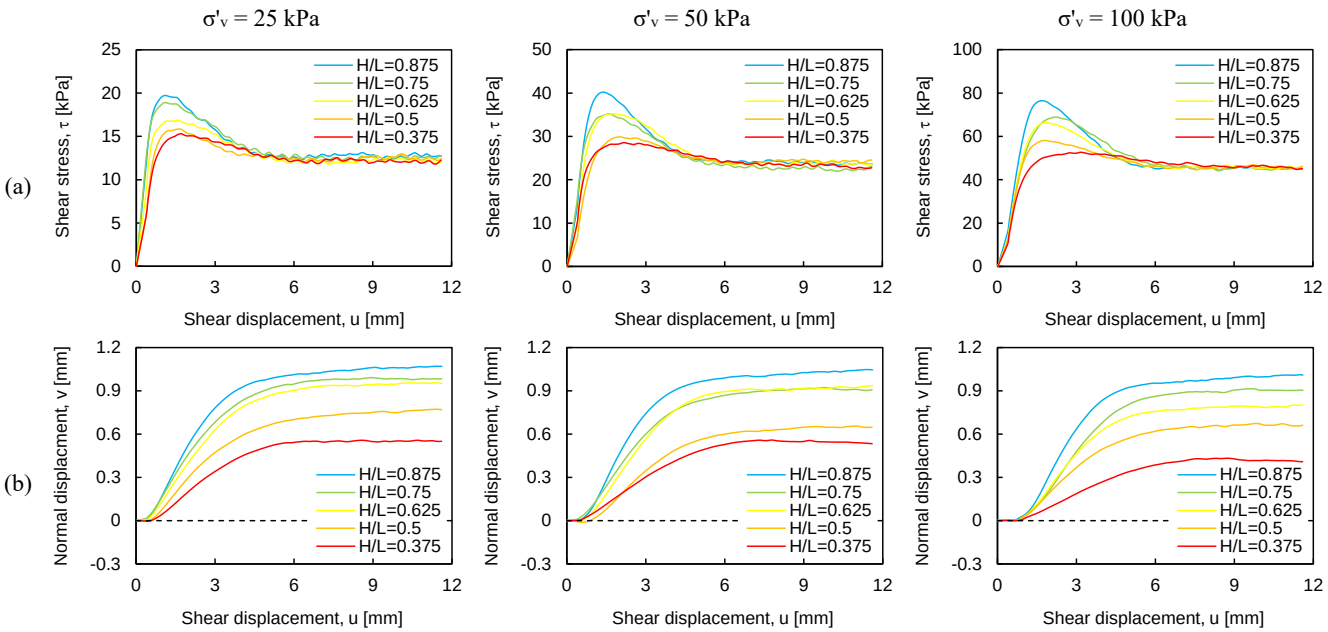

Fig. 3 Experimental results according to aspect ratio: (a) Shear stress vs. shear displacement and (b) Normal displacement vs. shear displacement

terminology for the critical state as a criterion for determining whether the soil specimen expands or contracts upon shearing. Roscoe *et al.* (1958) defined the critical state as the state in which the stress and void ratio of a soil specimen remain constant under continuous deformation. The friction angle at the critical state (ϕ'_{crit}) is independent of the initial void ratio, confining stress, and shearing rate. When a soil specimen is sheared under a constant confining stress, its void ratio converges to a specific value regardless of the initial void ratio under large shear displacements (Wroth 1958). A consistent friction angle at a large shear displacement, independent of the specimen height, caused negligible volume change (Fig. 3). Therefore, the residual state, which indicates that the specimen is sheared at large deformations, must be considered as a critical state. In this study, the friction angles at large displacements were calculated by averaging the values corresponding to the shear displacements between 10 and 12 mm. As shown in Fig. 4(b), the representative value of the residual friction angle (ϕ'_{res}) is 24.73° regardless of the confining stress and

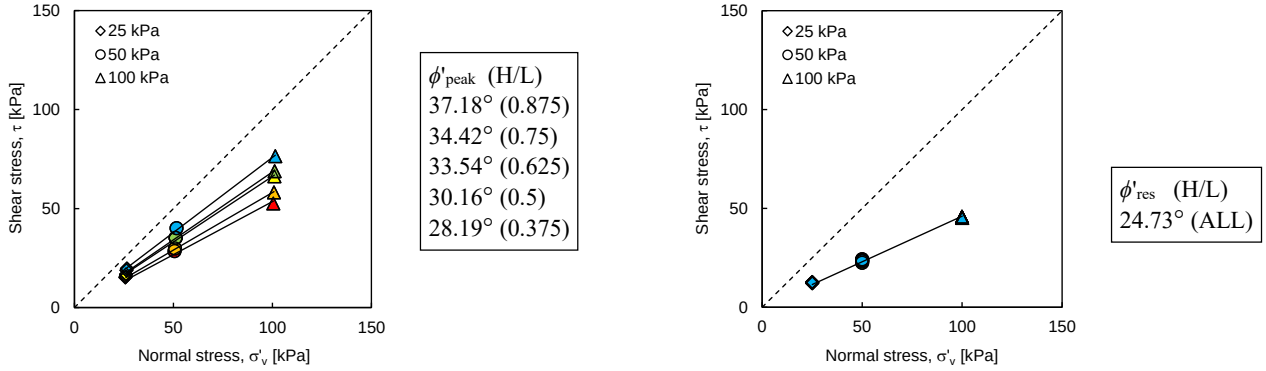

(a) Peak friction angle (b) Residual friction angle

Fig. 4 Friction angles obtained by Mohr-Coulomb failure envelop

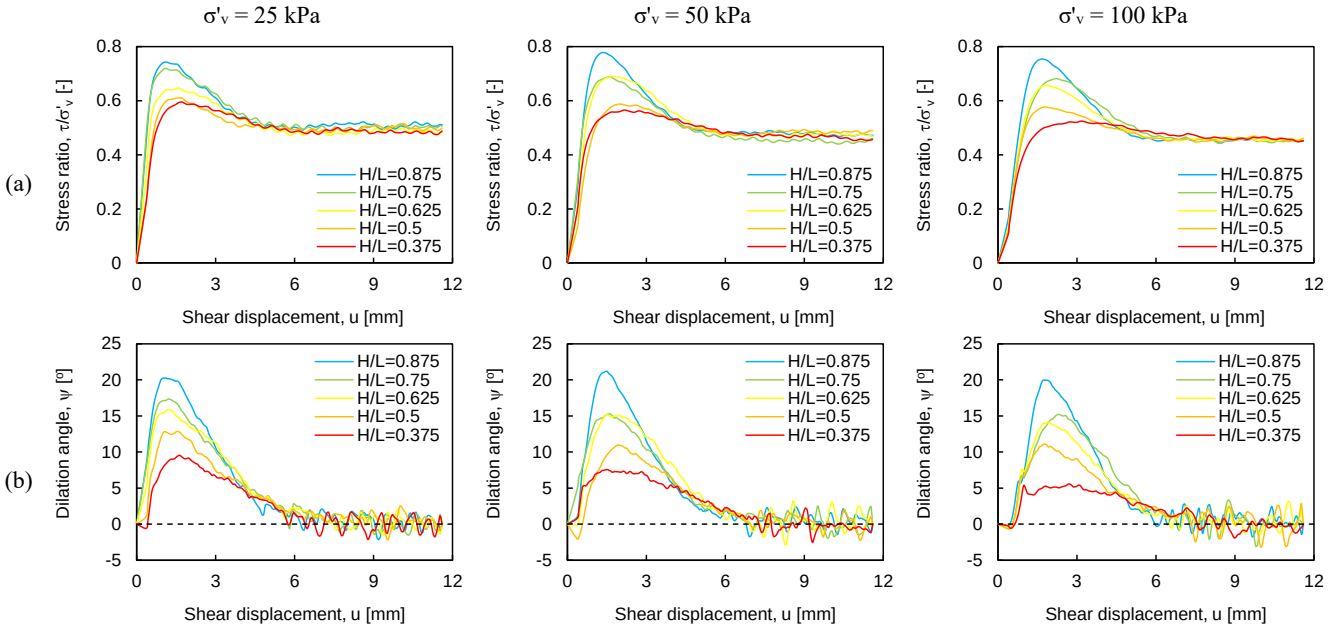

Fig. 5 Experimental results according to aspect ratio: (a) Stress ratio vs. shear displacement and (b) Dilation angle vs. shear displacement

specimen height.

The evaluation of shear behavior is indispensable for solving geotechnical engineering problems such as those related to foundations, sheet piling, retaining walls, and slope stability. It includes the prediction of the deformation characteristics occurring during the shearing process, as well as the resistance to shear failure. To understand the shear strength of soils, the friction angle and dilatancy cannot be considered separately because they are closely related. Taylor (1948) stated that the shear strength of soils can be expressed by combining two parameters: the friction angle (ϕ') and dilation angle (ψ), representing resistance and deformation, respectively. The direct shear friction angle (ϕ'_{ds}) with the vertical stress (σ'_{yy}) and shear stress (τ'_{yx}) measured at the boundary of the shear box is expressed by Eq. (1). The dilation angle (ψ) with increasing vertical displacement (v) and horizontal displacement (u) can be obtained using Eq. (2)

$$\phi'_{ds} = \frac{\tau_{yx}}{\sigma'_{yy}} \tag{1}$$

$$\tan\psi = \frac{d\varepsilon_{yy}}{d\gamma_{yx}} = \frac{dv}{du} \tag{2}$$

where the subscript ds indicates direct shear and ϕ'_{ds} indicates the friction angle obtained by the direct shear test. In Eq. (1), the ratio of shear stress to vertical stress (τ/σ'_y) is called the stress ratio (SR). The relationship between the stress ratio and shear displacement is shown in Fig. 5(a). The shear stress corresponding to the shear displacement is shown in Fig. 3(a), where a higher stress ratio is observed for the specimen with a higher aspect ratio (H/L). Moreover, the stress ratio in the residual state had virtually the same value, regardless of the aspect ratio.

As mentioned previously, the dilation angle (ψ) is an

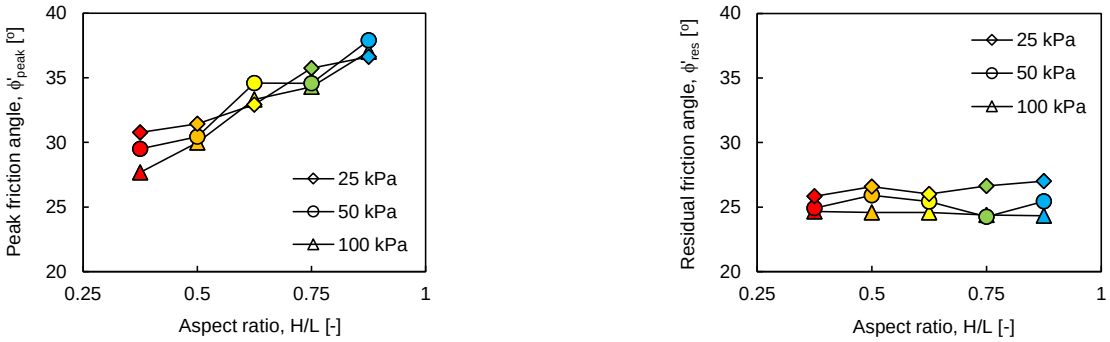

(a) Peak friction angle (b) Residual friction angle

Fig. 6 Relationship between aspect ratio and friction angle

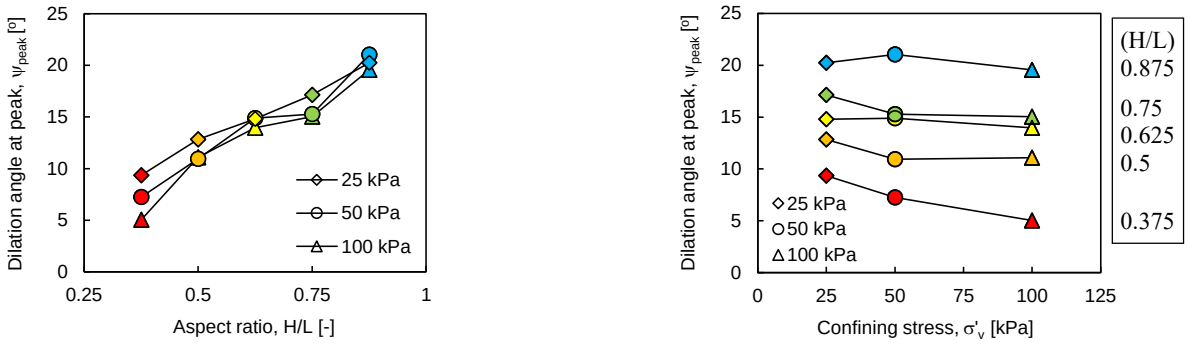

(a) Aspect ratio (b) Confining stress

Fig. 7 Variation of the dilation angle at peak shear strength

expression of the volume change in a specimen during a direct shear test. The dilation angles obtained using Eq. (2) along the shear displacement are shown in Fig. 5(b). Initially, the angle had a negative value; then, it increased rapidly to its maximum value. The shear displacement when the dilation angle reaches the maximum value is virtually identical to that of the maximum stress ratio, which is referred to as u_{peak}. After reaching the maximum, the dilation angle decreases to zero at a shear displacement value of approximately 8–9 mm at large displacements, and fluctuates near zero. This is consistent with the previous results, which showed that no considerable volume change occurred in the residual state.

5. Analysis and discussion

5.1 Resistance characteristics

Based on the descriptions listed in Table 2, the peak friction angles (ϕ'_{peak}) and residual friction angles (ϕ'_{res}) are shown in Fig. 6 with different aspect ratios (H/L). As shown in Fig. 6(a), the peak friction angle gradually increased with the height of the specimen. When the aspect ratio was 0.375, the friction angle was approximately 30°. When the aspect ratio was 0.875, the peak friction angle exceeded 35°. The residual friction angle presented a uniform range of values between 24° and 27°, regardless of the height of the specimen (Fig. 6(b)). Stroud (1971) and Lings and Diez (2004) reported that the friction angle at the critical state decreases with increasing confining stress. Furthermore, a numerical analysis conducted by El-Emam *et al.* (2012) using the finite-difference method showed that the friction angle was dependent on the stress level. In agreement with previous studies, some irregularities were observed; however, both angles tended to decrease as the stress increased. In particular, the residual friction angle, which is generally considered to be unaffected by the confining stress, has also been experimentally proven to be dependent on stress.

The dilation angle at the peak (ψ_{peak}) when the shear strength was at its peak is shown in Fig. 7. The dilation angles for different aspect ratios (H/L) are shown in Fig. 7(a). The figure indicates that the dilation angle increased linearly with H/L; however, it decreased slightly with increasing confining stress, as shown in Fig. 7(b). The effects of height scale and confining stress on the dilation angle at the peak shear strength were the same as those at the peak friction angle. These observations can be inferred from the close relationship between friction and dilation angles.

5.2 Deformation characteristics

As previously mentioned, friction angle and dilatancy are closely related. Several studies have clarified this relationship, known as the flow rule. Taylor (1948) presented an energy-based analysis and experimentally demonstrated that dilatancy was stress-dependent (Taylor 1948, Bishop 1950). Rowe (1962) expressed the stress-

dilatancy theory for the plane strain. This relationship is expressed by Eq. (3)

$$R = DK \text{ or } \frac{\sigma_1'}{\sigma_3'} = \left(\frac{-\mathrm{d}\varepsilon_3}{\mathrm{d}\varepsilon_1}\right)\tan^2\left(45+\phi_{\mathrm{crit}}'/2\right) \quad (3)$$

where the subscript crit is the critical state; hence, ϕ'_{crit} indicates the friction angle at a critical state. Several theoretical flow rules have been derived from coaxiality (Hill 1950), which assumes that the directions of the principal stresses and principal strain increments coincide with the structural similarity (Cole 1967, Roscoe *et al.* 1967, Davis 1968, Rowe 1969). Bolton (1986) presented a simple empirical equation derived from experimental data and not from a theoretical approach. The derived equation is as follows

$$\phi_{ps}' = \phi_{ps,crit}' + 0.8\psi \quad (4)$$

where the subscript ps denotes plane strain; hence, ϕ'_{ps} indicates the friction angle under plane strain condition. Lings and Dietz (2004) and Simoni and Houlsby (2006) reviewed the validity of Eq. (4), based on the experimental tests. Moreover, they compared and analyzed the various equations presented above. Simoni and Houlsby (2006) proposed Eq. (5), which removed the ϕ'_{ps} terms for interpreting the results obtained using the direct shear test. The proposed equation is as follows

$$\phi_{ds,peak}' - \phi_{ds,crit}' = b\psi_{peak} \quad (5)$$

where ψ_{peak} denotes the dilation angle corresponding to the peak shear strength. Moreover, the coefficient *b* is a function of ϕ'_{crit} and ψ and is not a constant. Nevertheless, it can be considered to be nearly constant because the variation in b is negligible.

Based on Eq. (5) (Simoni and Houlsby 2006), Fig. 8 shows the relationship between friction and dilation angles. The group of symbols on the left side of the graph near the zero-dilation angle shows the residual friction and the dilation angles (obtained by averaging those corresponding to the shear displacement from 10 to 12 mm). The other symbols plot the peak friction angle and corresponding dilation. Residual friction angle data were excluded from the linear regression analysis. After collecting 15 test results, a linear regression line was obtained using Eq. (6)

$$\phi_{ds,peak}' = 0.64\psi_{peak} + 24.17 \quad (6)$$

By comparing Eqs. (5) and (6), gradient *b* was determined to be 0.64. The intercept, $\phi'_{ds,crit}$, is 24.17° with a coefficient of determination (R^2) of 0.95. Guo and Su (2007) reported *b* values of 0.63 and 0.91 in the experimental tests conducted on rounded and angular particles, respectively. The value of 0.63 on rounded particles was similar to the value of 0.64 obtained using glass beads in this study. Hence, the peak friction angle is linearly proportional to the dilation angle regardless of the aspect ratio.

The results presented in Section 5.1 indicate that the peak friction angle (ϕ'_{peak}) and dilation angle at the peak (ψ_{peak}) linearly increase with the aspect ratio (H/L), and the

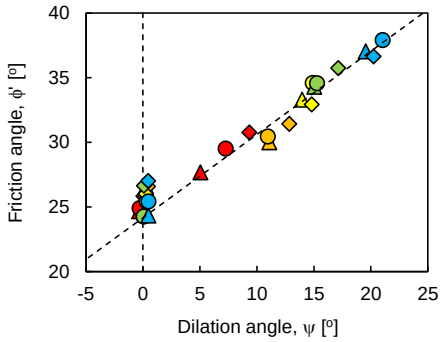

Fig. 8 Relationship between dilation angle and peak friction angle

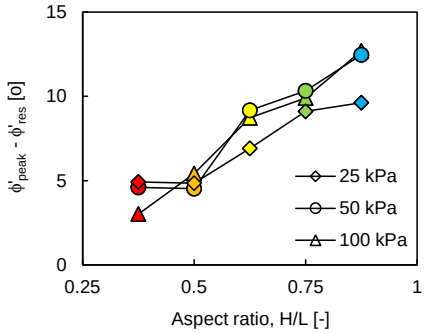

Fig. 9 Difference between peak friction angle and residual friction angle according to aspect ratio

residual friction angle (ϕ'_{res}) remains relatively constant. As expressed in Eq. (5) because the difference between the peak and residual friction angles is linearly proportional to the dilation angle at the peak, the difference between the peak and residual friction angles can be predicted relative to the aspect ratio. Therefore, the differences are presented in terms of the aspect ratio in Fig. 9. As expected, the difference between the peak and residual friction angles linearly increased with the aspect ratio.

5.3 Stiffness characteristics

This section presents an investigation of the stiffness characteristics in the direct shear test with respect to the aspect ratio (H/L) and confining stress (σ'_v). Identifying stiffness characteristics facilitates the prediction of the maximum allowable strain in geotechnical problems. The shear modulus (G) of soils indicates the slope of the stress-strain curve and can be calculated using Eq. (7)

$$G = \frac{\tau}{\gamma} \quad (7)$$

where γ denotes the shear strain. The shear strain can be calculated by dividing the shear displacement by the height (the height does not denote the total height of the specimen; it is the height of the shear area in which the actual shear deformation occurs). A value corresponding to half the total height of a specimen is typically used as the thickness of the shear zone (Head 2011). However, the thickness of the shear zone is affected by various factors such as the particle size distribution, confining stress, and angularity. In this

study, the shear zone thickness varied considerably depending on specimen height. Accordingly, instead of a vague concept of shear strain, a simple and intuitive shear deformation (u) concept was used in this study.

A simple method for obtaining the stiffness features from a direct shear test is to divide the peak shear stress (τ_{peak}) by the corresponding shear displacement (u_{peak}). However, prior to this, the shear displacement at the peak must be examined, as shown in Fig. 10. The shear displacement at the peak decreased with an increase in the aspect ratio, as shown in Fig. 10(a). A small value of shear displacement at the peak indicates that the shear strength rapidly reached the peak state, implying that the stiffness of the specimen was considerable. Although all the specimens were prepared with the same initial void ratio (e_0), the local void ratio around the shear zone depends on the confining stress and height scale during shearing. Hence, a loose bulk density appeared in the shear zone when the aspect ratio was high and confining stress was low. This is consistent with the dilation-angle results shown in Fig. 7. Hence, a small dilation angle creates a dense layer around the shear zone. This indicates that the specimen had a high stiffness, and eventually, the maximum shear strength was rapidly reached. However, Wang and Gutierrez (2010) reported the opposite: the higher the aspect ratio, the greater the shear displacement at the peak. In the current study, all the specimens had the same initial void ratios. In contrast, the void ratio of the specimens used by Wang and Gutierrez (2010) varied depending on the specimen height. Owing to the large height of the specimen with a lower void ratio, the shear displacement at the peak must increase. The secant modulus was determined by dividing the shear stress at the peak shear strength (τ_{peak}) by the corresponding shear displacement at the peak (u_{peak}), as shown in Fig. 11(a). Consequently, the secant modulus (τ_{peak}/u_{peak}) increased with aspect ratio and confining stress.

In general, the shear modulus decreased gradually as the shear strain increased. Although it is not sufficient to compare the G_{max} values at extremely small shear strains (less than 10^{-5}), the secant shear modulus used in this study can also be advantageous for comparing the effect of height scale on shear stiffness. The maximum values of the shear moduli (i.e., the slope at the beginning of the shear stress–shear displacement curve) are shown in Fig. 11(b). The maximum value of the tangent shear modulus also increases with the aspect ratio (H/L). In addition, the tangent modulus exhibited a large value when the confining stress was high. However, the stiffness characteristics based on the shear stress shown in Fig. 11 do not consider the influence of the confining stress. It was necessary to normalize and compare the stiffness characteristics based on the aspect ratio. Three methods are commonly used to normalize the shear modulus (G) are commonly used. The first involves dividing the shear modulus by the average effective stress (p') (Pantelidou and Simpson 2007, Hight *et al.* 2007, Grammatikopoulou *et al.* 2008). The second method divides the shear modulus by the undrained shear strength (C_u) (Butler 1975, Hewitt 1989). In the third method, the shear modulus is divided by G_{max}. Among the three methods, the third, which uses G_{max}, is known to be the most effective in

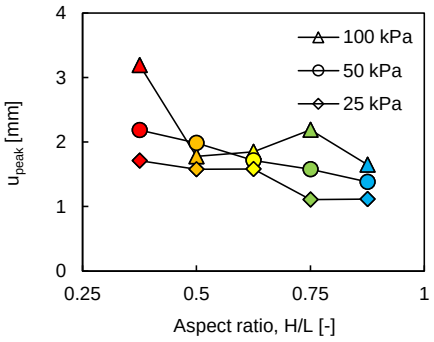

Fig. 10 Variation of shear displacement at the peak shear strength (u_{peak}) according to aspect ratio

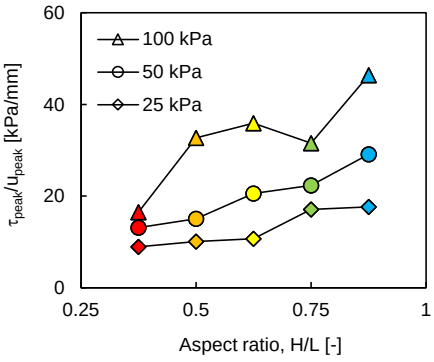

(a) τ_{peak}/u_{peak}

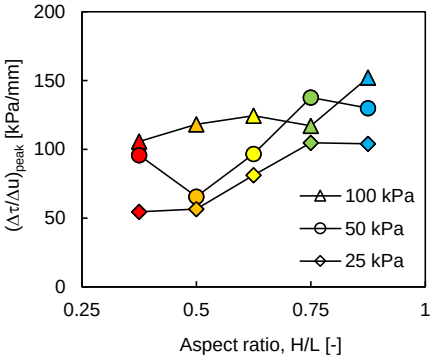

(b) $(\Delta\tau/\Delta u)_{peak}$

Fig. 11 Shear stiffness characteristics according to aspect ratio

reducing scatter. However, G_{max} could not be derived using a direct shear test. The second method, the undrained shear strength test, which is a drainage test, is not suitable for this study. Moreover, it is difficult to use the first method because the rotation of the principal stress direction imposed by direct shearing is not accurately known. Therefore, in this study, a normalizing method was employed to divide the shear stress by the confining stresses.

The secant shear modulus calculated by dividing the peak stress ratio $(\tau/\sigma'_v)_{peak}$ by the corresponding shear displacement is shown in Fig. 12(a). The modulus increased with confining stress and decreased with increasing aspect ratio. However, the results shown in Fig. 12(a) do not reflect the maximum slope of the stress ratio-shear displacement curve. Similar to Fig. 11(b), the maximum

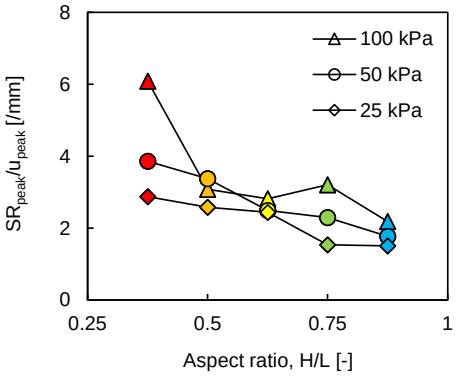

(a) SR_{peak}/u_{peak}

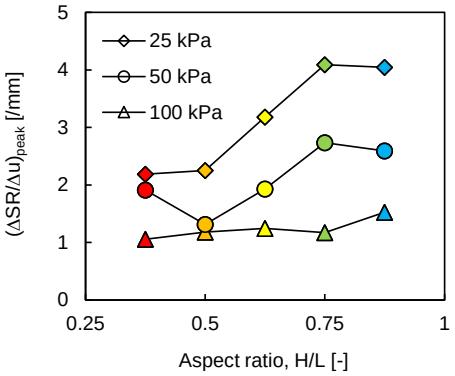

(b) $(\Delta SR/\Delta u)_{peak}$

Fig. 12 Normalized shear stiffness characteristics according to aspect ratio

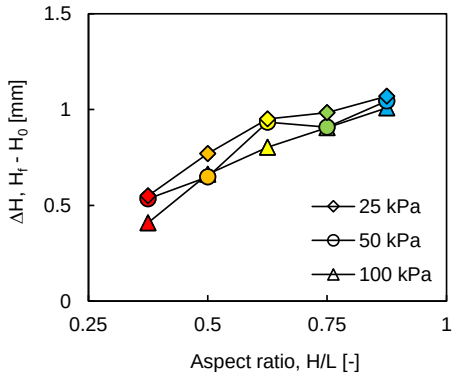

(a) Specimen height

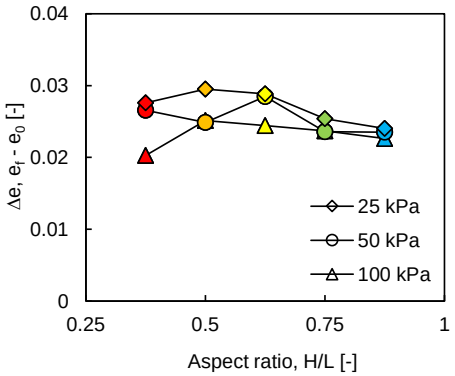

(b) Void ratio

Fig. 13 Total change in specimen height and void ratio according to aspect ratio

values of the shear modulus determined from the initial slope of the curve are plotted in Fig. 12(b). In contrast to Fig. 12(a), Fig. 12(b) indicates that the stiffness increases with the aspect ratio, and the lower the confining stress, the greater the stiffness.

5.4 Effect of DSB height scale

This section presents the changes in the heights of the specimen with respect to the aspect ratio (H/L). Moreover, the development of the shear zone was discussed. The volume change in the actual shear zone is considerably greater than the values measured at the boundary (Thornton and Zhang 2003, Zhang and Thornton 2007, He *et al*. 2021, Nitka and Grabowski 2021). Therefore, ASTM D3080 recommends that the aspect ratio (H/L) should not exceed 0.5. However, Fig. 13(a) shows that the total change in specimen height (ΔH) increases linearly with the aspect ratio. Furthermore, the total change in the void ratio (Δe) exhibited a similar value regardless of the aspect ratio, as shown in Fig. 13(b). In particular, it converges in the case of high aspect ratios (i.e., 0.75 and 0.875) and finally exhibits a uniform distribution. Therefore, the aspect ratio does not significantly affect the total change in void ratio (Δe). The changes in the height and void ratio shown in Figs. 13(a) and 13(b), respectively, indicate the global value in the specimen and not the local value in the actual shear zone.

The development of the shear zone is affected by void ratio, confining stress, and particle size distribution (Saada *et al*. 1999). Zhang and Thornton (2007) reported that the greater the height of the specimen, the larger is the number of particles involved in the shear behavior up to the peak shear strength, which causes more external forces to act on the specimen. In conclusion, the higher the height of the sample, the thicker the shear zone developed. Furthermore, an increase in the number of particles involved in shear behavior results in an increase in the shear resistance of the sample.

In the direct shear test, the vertical and shear stresses were determined directly from a potential shear plane; however, these may not represent the maximum stress ratios inside the specimen. Furthermore, the magnitudes of the principal stresses were unknown, and their directions were assumed. An inevitable problem in this study was the change in H/D_{max} from 30 to 70 owing to the change in the specimen height without any changes in its length. In this study, with no consideration of these uncertainties, interpretation of the results using a type-C shear box was performed to evaluate the scale effect on the shear behavior. The purpose of this study was not to determine the appropriate aspect ratio. Because no shear zone was observed, it was difficult to determine the appropriate aspect ratio. Nevertheless, the foregoing supports the discussions on the type and size criteria for the shear box in direct shear tests.

6. Conclusions

In this study, the effect of the height scale of a shear box on the shear behavior of dilative granular materials was evaluated using a direct shear test with a type-C shear box. The five shear boxes had different aspect ratios (H/L) (0.375, 0.5, 0.625, 0.75, and 0.875) with heights ranging from 30 to 70 mm; the length was fixed at 80 mm. In all the tests, the specimens were composed of glass beads with an initial void ratio of 0.540 ± 0.003 before shearing. Experimental tests were performed by applying three constant confining stresses: 25, 50, and 100 kPa. Through 15 tests, the effect of the height scale on the resistance and deformation of the dilative granular materials was analyzed. Furthermore, the stiffness characteristics were investigated, the volume changes in the specimens were evaluated, and the development of the shear zone was discussed. The main observations and conclusions of this study are as follows:

The dilation angle at the peak (ψ_{peak}) linearly increases with the aspect ratio, and the increment in ψ_{peak} is reflected in the peak friction angle (ϕ'_{peak}); however, the residual friction angle remains relatively constant. In addition, the shear displacement at the peak decreases with increasing aspect ratio, indicating considerable stiffness. The height of the specimen did not significantly affect the change in the void ratio, and the final void ratio gradually converges as the height increases. As the height of the specimen increased, the number of particles involved in the shear behavior increased, causing an additional external shear force to act on the specimen. In conclusion, the results of this study indicate that a higher aspect ratio results in a thicker shear zone and higher resistance. Although H/D_{max} is not constant owing to the change in specimen height, the interpretations and results show the scale effect on the shear behavior using a type-C shear box. This study is expected to benefit the research on the criteria for the shear-box scale in direct shear tests.

Acknowledgments

This research was supported by the Korea Agency for Infrastructure Technology Advancement under the Ministry of Land, Infrastructure and Transport of the Korean government (Project Number: 22UGCP-B157945-03).

References

ASTM D3080/D3080M-11. (2011), *Standard Test Method for Direct Shear Test of Soils Under Consolidated Drained Conditions*, ASTM International, West Conshohocken, PA, USA.

Beren, M., Cobanoglu, I., Çelik, S.B. and Ündül, Ö. (2020), "Shear rate effect on strength characteristics of sandy soils", *Soil Mech. Found. Eng.*, **57**, 281-287. https://doi.org/10.1007/s11204-020-09667-y.

Bishop, A.W. (1950), "Discussion on measurement of shear strength of soils", *Géotechnique*, **2**(1), 113-116.

Bolton, M.D. (1986), "The strength and dilatancy of sands", *Géotechnique*, **36**(1), 65-78. https://doi.org/10.1680/geot.1986.36.1.65.

Butler, F.G. (1975), "General report and state-of-the-art review—Session 3", *Proceedings of the Conference on Settlement of Structures*, Pentech Press, London.

Casagrande, A. (1936), "The determination of the pre-consolidation load and its practical significance", *Proceedings of the 1st International Conference on Soil Mechanics and Foundation Engineering*, Cambridge, MA, June.

Cerato, A.B. and Lutenegger, A.J. (2006), "Specimen size and scale effects of direct shear box tests of sands", *Geotech. Test. J.*, **29**(6), 507-516. https://doi.org/10.1520/GTJ100312.

Cerato, A.B., and Lutenegger, A.J. (2007), "Scale effects of shallow foundation bearing capacity on granular material", *J. Geotech. Geoenviron. Eng.*, **133**(10), 1192-1202. https://doi.org/10.1061/(ASCE)1090-0241(2007)133:10(1192).

Cole, E.R.L. (1967), "The behaviour of soils in the simple shear apparatus", Ph.D. Dissertation, University of Cambridge, Cambridge.

Davis, E.H. (1968), "Theories of plasticity and failure of soil masses", *Soil mechanics: selected topics* (Ed., I.K. Lee), 341-354. New York, NY, USA.

Deiminiat, A., Li, L. and Zeng, F. (2022), "Experimental study on the minimum required specimen width to maximum particle size ratio in direct shear tests", *Civil Eng.*, **3**(1), 66-84. https://doi.org/10.3390/civileng3010005.

El-Emam, M., Attom, M. and Khan, Z. (2012), "Numerical prediction of plane strain properties of sandy soil from direct shear test", *Int. J. Geotech. Eng.,* **6**(1), 79-90. https://doi.org/10.3328/IJGE.2012.06.01.79-90.

Grammatikopoulou, A., Zdravkovic, L. and Potts, D.M. (2008), "The influence of previous stress history and stress path direction on the surface settlement trough induced by tunnelling", *Géotechnique*, **58**(4), 269-281. https://doi.org/10.1680/geot.2008.58.4.269.

Guo, P., and Su, X. (2007), "Shear strength, interparticle locking, and dilatancy of granular materials", *Can. Geotech. J.*, **44**(5), 579-591. https://doi.org/10.1139/t07-010.

He, H., Zheng, J. and Schaefer, V.R. (2021), "Simulating shearing behavior of realistic granular soils using physics engine", *Granul. Matter.*, **23**, 1-20. https://doi.org/10.1007/s10035-021-01122-5.

Head, K.H. (1980), *Permeability, shear strength and compressibility tests*, Manual of soil laboratory testing 2, Pentech Press, London, England.

Hewitt, P. (1989), "Settlement of structures on overconsolidated clay", Master of Science Engineering Thesis, University of Sydney, Sydney, Australia.

Hight, D.W. and Leroueil, S. (2003), "Characterisation of soils for engineering purposes", *Characterisation and engineering properties of natural soils*, **1**, 255-360.

Hight, D.W., Gasparre, A., Nishimura, S., Minh, N.A., Jardine, R.J. and Coop, M.R. (2007), "Characteristics of the London Clay from the Terminal 5 site at Heathrow Airport", *Géotechnique*, **57**(1), 3-18. https://doi.org/10.1680/ssc.41080.0016.

Hill, R. (1950), *The mathematical theory of plasticity*, Oxford University Press, Oxford.

Jacobson, D.E., Valdes, J.R. and Evans, T.M. (2007), "A numerical view into direct shear specimen size effects", *Geotech. Test. J.*, **30**(6), 512-516. http://doi.org/10.1520/GTJ100923.

Jewell, R.A. and Wroth, C.P. (1987), "Direct shear tests on reinforced sand", *Géotechnique*, **37**(1), 53-68. https://doi.org/10.1680/geot.1987.37.1.53.

Jewell, R.A. (1989), "Direct shear tests on sand", *Géotechnique*, **39**(2), 309-322. https://doi.org/10.1680/geot.1989.39.2.309.

Kim, B.S., Shibuya, S., Park, S.W. and Kato, S. (2012), "Effect of opening on the shear behavior of granular materials in direct shear test", *KSCE J. Civ. Eng.*, **16**, 1132-1142.

https://doi.org/10.1007/s12205-012-1518-4.
Kim, B.S. (2021), "Establishing an opening size criterion in direct shear test using DEM Simulation", *Geomech. Eng.*, **26**(2), 147-160. https://doi.org/10.12989/gae.2021.26.2.147.
Kögler, D.P. and Scheidig, A. (1938), *Baugrund und Bauwerk*, Wilhelm Ernst und Sohn, Berlin.
Lings, M.L. and Dietz, M.S. (2004), "An improved direct shear apparatus for sand", *Géotechnique*, **54**(4), 245-256. https://doi.org/10.1680/geot.2004.54.4.245.
Mikasa, M. (1960), "New direct shear test apparatus", *Proceedings of the 15th Annual Conferenc*e of JSCE, Tokyo.
Nitka, M. and Grabowski, A. (2021), "Shear band evolution phenomena in direct shear test modelled with DEM", *Powder Technol*., **391**, 369-384. https://doi.org/10.1016/j.powtec.2021.06.025.
Palmeira, E.M. and Milligan, G.W.E. (1989), "Scale effects in direct shear tests on sand", *Proceedings of the 12th International Conference on Soil Mechanics and Foundation Engineering*, Rio de Janeiro, August.
Pantelidou, H. and Simpson, B. (2007), "Geotechnical variation of London Clay across central London", *Géotechnique*, **57**(1), 101-112. https://doi.org/10.1680/geot.2007.57.1.101.
Parsons, J.D. (1936), "Progress report on an investigation of the shearing resistance of cohesionless soils", *Proceedings of the 1st International Conference on Soil Mechanics and Foundation Engineering*, 2, Cambridge, June.
Roscoe, K.H., Schofield, A. and Wroth, A.P. (1958), "On the yielding of soils", *Géotechnique*, **8**(1), 22-53. https://doi.org/10.1680/geot.1958.8.1.22.
Roscoe, K.H. (1967), "Principal axes observed during simple shear of a sand". *Proceedings of the Geotechnical Conference on Geotechnical Properties of Natural Soils and Rocks*, Norwegian Geotechnical Society, Oslo, Norway.
Rowe, P.W. (1962), "The stress-dilatancy relation for static equilibrium of an assembly of particles in contact", *Proceedings of the Royal Society of London. Series A. Mathematical and Physical Sciences*, **269**(1339), 500-527. https://doi.org/10.1098/rspa.1962.0193.
Rowe, P.W. (1969), "The relation between the shear strength of sands in triaxial compression, plane strain and direct", *Géotechnique*, **19**(1), 75-86. https://doi.org/10.1680/geot.1969.19.1.75.
Saada, A.S., Liang, L., Figueroa, J.L. and Cope, C.T. (1999), "Bifurcation and shear band propagation in sands", *Géotechnique*, **49**(3), 367-385. https://doi.org/10.1680/geot.1999.49.3.367.
Scaringi, G. and Di Maio, C. (2016), "Influence of displacement rate on residual shear strength of clays", *Procedia Earth Planet. Sci.*, **16**, 137-145. https://doi.org/10.1016/j.proeps.2016.10.015.
Scarpelli, G. and Wood, D.M. (1982), "Experimental observations of shear patterns in direct shear tests", *IUTAM Deformation and Failure of Granular Materials Conference*, Delft, August.
Shibuya, S., Mitachi, T. and Tamate, S. (1997), "Interpretation of direct shear box testing of sands as quasi-simple shear", *Géotechnique*, **47**(4), 769-790. https://doi.org/10.1680/geot.1997.47.4.769.
Simoni, A. and Houlsby, G.T. (2006), "The direct shear strength and dilatancy of sand-gravel mixtures", *Geotech. Geol. Eng.*, **24**, 523-549. https://doi.org/10.1007/s10706-004-5832-6.
Skempton, A.W. and Bishop, A.W. (1950), "The measurement of the shear strength of soils", *Géotechnique*, **2**(2), 90-108. https://doi.org/10.1680/geot.1950.2.2.90.
Stone, K.J.L. and Wood, D.M. (1992), "Effects of dilatancy and particle size observed in model tests on sand", *Soils Found.*, **32**(4), 43-57. https://doi.org/10.3208/sandf1972.32.4_43.
Stroud, M.A. (1971), "The behaviour of sand at low stress levels in the simple-shear apparatus", Ph.D. Dissertation, University of Cambridge, Cambridge.
Takada, N. (1993), "Mikasa's direct shear apparatus, test procedures and results", *Geotech. Test. J.*, **16**(3), 314-322. https://doi.org/10.1520/GTJ10052J.
Taylor, D.W. (1948), *Fundamentals of soil mechanics*, John wiley & Son, New York.
Thornton, C. and Zhang, L. (2003), "Numerical simulations of the direct shear test", *Chem. Eng. and Technol.*, **26**(2), 153-156. https://doi.org/10.1002/ceat.200390022.
Tika, T.E., Vaughan, P.R. and Lemos, L.J. (1996), "Fast shearing of pre-existing shear zones in soil", *Géotechnique*, **46**(2), 197-233. https://doi.org/10.1680/geot.1996.46.2.197.
Vermeer, P.A. (1990), "The orientation of shear bands in biaxial tests", *Géotechnique*, **40**(2), 223-236. https://doi.org/10.1680/geot.1990.40.2.223.
Wang, J. and Gutierrez, M. (2010), "Discrete element simulations of direct shear specimen scale effects", *Géotechnique*, **60**(5), 395-409. https://doi.org/10.1680/geot.2010.60.5.395.
Wroth, C.P. (1958), "The behaviour of soils and other granular media when subjected to shear", Ph.D. Dissertation, University of Cambridge, Cambridge.
Wu, P.K., Matsushima, K. and Tatsuoka, F. (2008), "Effects of specimen size and some other factors on the strength and deformation of granular soil in direct shear tests", *Geotech. Test. J.*, **31**(1), 45-64. https://doi.org/10.1520/GTJ100773.
Zhang, L. and Thornton, C. (2007), "A numerical examination of the direct shear test", *Géotechnique*, **57**(4), 343-354. https://doi.org/10.1680/geot.2007.57.4.343.
Zhou, Q., Shen, H.H., Helenbrook, B.T. and Zhang, H. (2009), "Scale dependence of direct shear tests", *Chin. Sci. Bull.*, **54**, 4337-4348. https://doi.org/10.1007/s11434-009-0516-5.

GC